Static and dynamic properties of grafted ring polymer: Molecular dynamics simulation

2013 Chinese Phys. B 22 016101

(http://iopscience.iop.org/1674-1056/22/1/016101)

Static and dynamic properties of grafted ring polymer: Molecular dynamics simulation*

He Su-Zhen(何素贞)[a)b)], Holger Merlitz(候 格)[a)c)], Su Chan-Fei(苏婵菲)[a)], and Wu Chen-Xu(吴晨旭)[a)†]

[a)] *Department of Physics and ITPA, Xiamen University, Xiamen* 361005, *China*
[b)] *Department of Electronic Engineering, Putian University, Putian* 351100, *China*
[c)] *Leibniz-Institut fürPolymerforschung Dresden, Dresden* 01069, *Germany*

(Received 18 June 2012; revised manuscript received 2 September 2012)

The static and dynamic properties of a system of end-grafted flexible ring polymer chains grafted to a flat substrate and exposed to a good solvent are studied by using a molecular dynamics method. The monomers are described by a coarse-grained bead-spring model. Varying the grafting density ρ and the degree of polymerization or chain length N, we obtain the density profiles of monomers, study the structural properties of the chain (radius of gyration, bond orientational parameters, etc.), and also present the dynamic characteristics such as chain energy and bond force. Compared with a linear polymer brush, the ring polymer brush exhibits different static and dynamic properties for moderate or short chain length, while it behaves like linear polymer brush in the regime of long chain length.

Keywords: ring polymer , molecular dynamics, scaling

PACS: 61.41.+e **DOI:** 10.1088/1674-1056/22/1/016101

1. Introduction

Polymer brushes consisting of end-grafted polymer chains will be stretched away from the substrate due to the volume-excluded effect, and also have important technological applications, including surface modification, colloidal stabilization, and lubrication.[1] Depending on chain length, grafting density and solvent quality, polymer brushes reveal a variety of statical and dynamical properties. Under suitable solvent conditions, polymer chains with one end attached to a flat surface will be stretched when the grafting density ρ is high enough to allow overlap between individual chains. The theoretical investigations of linear polymer brushes have been carried out widely with significant progress since the seminal work by Alexander[2] and de Gennes,[3] including the self-consistent field (SCF) theory,[4–7] which has been established as a powerful tool for a quantitative understanding of polymer brushes beyond scaling theory. The initial approaches were mostly based on the Gaussian chain approximation. However, for high grafting densities, when the chains become strongly stretched, the finite extensibility of chains has to be taken into account.[8–10] The conformations of polyelectrolyte brushes is also a topic of interest, both from the viewpoint of theory[11,12] and of molecular dynamics (MD) simulation.[13,14]

It is, therefore, of great interest to study polymers with topological architecture,[15] such as stars or rings. For these nonlinear architectures, predictions of different theories are typically very different. Thus, such studies offer a chance to test the validity of different theoretical approaches initially derived from linear polymers. A basis for the present understanding of the dynamics of a ring polymer has been built by Kahyun *et al.*,[16] in addition to the investigation on the adsorption of ring polymer onto a surface carried out by several groups both experimentally[17] and theoretically.[18,19]

In this paper, we present a computer simulation study of the equilibrium structures and dynamics of a ring polymer adsorbed on a surface. The comparison between the ring polymer brush and linear polymer brush in a good solvent is also carried out in our paper. The paper is organized as follows. On the basis of the simulation model introduced in Section 2, we carried out our simulation in Sections 3 and 4, where the equilibrium structure and dynamics of the polymer brush are analyzed and discussed. Compared with a linear polymer brush, our conclusion is presented in Section 5.

2. Simulation model

The bead-spring model for polymer chain was employed in our simulation. A single ring polymer chain was represented by a sequence of connective monomers. The ring polymer brush was modeled as a collection of freely jointed bead spring chains, anchored at one end to a planar surface to form a regular 8×8 square grid. Each chain was modeled as N spherical beads. The rectangular simulation box with a dimension of $L \times L \times L_z$ had periodic boundaries in both x (horizontal) and y directions. The molecular dynamics package LAMMPS[20] was used to carry out the simulations. In MD simulations, the Newton equations together with a random force are used, which is the core part of the Langevin equation. As the time steps we choose for simulation are small enough, overdamp-

*Project supported by the National Natural Science Foundation of China (Grant Nos. 50873083 and 10974162).
†Corresponding author. E-mail: cxwu@xmu.edu.cn

ing can be avoided, and a normal MD integrator can be used. Throughout this paper, Lennard–Jones (LJ) units were used. For unit style LJ, all quantities are unitless.[20] LAMMPS was used to set the fundamental quantities. The masses, distances, and energies we specify are multiples of these fundamental values. The total interaction potential is composed of three contributions

$$U_{\rm tot} = U_{\rm LJ} + U_{\rm FENE} + U_{\rm WALL}. \tag{1}$$

The chains were assumed to be in good solvent, modeled by a purely repulsive short-range Lennard–Jones potential, cut at its minimum

$$U_{\rm LJ}(r) = 4\varepsilon\Big[\Big(\frac{d}{r}\Big)^{12} - \Big(\frac{d}{r}\Big)^{6} - \Big(\frac{d}{r_{\rm c}}\Big)^{12} + \Big(\frac{d}{r_{\rm c}}\Big)^{6}\Big], \tag{2}$$

where ε is the potential depth, r is the distance between the particles, and $r_{\rm c} = 2^{1/6}d$ (with d being the size of the bead) is the cutoff radius. Apparently, conformations of polymer brushes depend on solvent qualities. In a good solvent, interactions between polymer segments and solvent molecules are favorable, and the loss of entropy of the chains on overlap will cause polymer chains to expand. Under different solvent conditions, polymer brushes will exhibit different behaviors, such as a scaling law. Neighboring beads along the polymer chains were coupled by a finitely extensible nonlinear elastic (FENE) bond potential[21]

$$\begin{aligned} U_{\rm FENE} \;=\; & -0.5kB^2\ln\Big[1-\Big(\frac{b}{B}\Big)^2\Big] \\ & +4\varepsilon\Big[\Big(\frac{d}{b}\Big)^{12} - \Big(\frac{d}{b}\Big)^{6}\Big] + \varepsilon, \end{aligned} \tag{3}$$

where the spring constant $k = 30\varepsilon/d^2$, b is the length of the bond, and the maximum bond length $B = 1.5d$. For the chains simulated in this paper, this parameter set delivered an average bond length of $l_{\rm av} = 0.98d$. There are two walls in the system, one located at $z = 0$, the same height as the substrate to which the chains were grafted, and the other at $z = L_z$. The coupling between polymer chains and the two walls was modeled as a 9–3 LJ potential

$$U_{\rm WALL} = \varepsilon\Big[\frac{2}{15}\Big(\frac{d}{z}\Big)^{9} - \Big(\frac{d}{z}\Big)^{3}\Big]. \tag{4}$$

The motion of monomers was governed by the Langevin equation

$$m\frac{{\rm d}^2\boldsymbol{r}_i}{{\rm d}t^2} + \varsigma\frac{{\rm d}\boldsymbol{r}_i}{{\rm d}t} = -\frac{\partial U_{\rm TOT}}{\partial \boldsymbol{r}_i} + \boldsymbol{F}_i, \tag{5}$$

where $m = 1$ is the monomer mass, $\boldsymbol{r}_i$ is the position of the i-th monomer, and ς is the friction constant. The $\boldsymbol{F}_i$ is a Gaussian random force that was used to couple the system to the heat bath, with the correlation function defined as

$$\langle \boldsymbol{F}_i(t)\cdot\boldsymbol{F}_j(t')\rangle = 2k_{\rm B}T\varsigma\delta_{ij}\delta_{\alpha\beta}\,. \tag{6}$$

The diameter of monomer is $d_{\rm mono} = 1.0$, and the temperature is $k_{\rm B}T = 1.2\varepsilon$, with $k_{\rm B}$ being the Boltzmann constant, and T the absolute temperature. Each time step is set at $\Delta t = 0.0015\tau_{\rm LJ}$, with $\tau_{\rm LJ} = (md^2/\varepsilon)^{1/2}$ being the Lennard–Jones time. The friction constant $\varsigma = \tau_{\rm LJ}^{-1}$ was used in our simulation. The initial brush conformation was set up as an array of stretched chains before their relaxation, for which 6×10^7 simulation steps were implemented. Figure 1 displays a typical ring polymer brush conformation after sufficient relaxation. In our simulation, the model is set to avoid self-knots and concatenations.

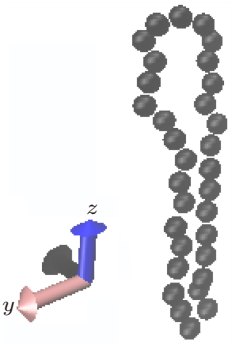

Fig. 1. (color online) Typical ring polymer brush conformation with 32 monomers in one chain.

3. MD simulation results and discussion

3.1. Equilibrium structure

In our simulations, a number of quantities were calculated. The size of a linear chain can be characterized by its mean-square end-to-end distance

$$\langle R^2\rangle = \langle \boldsymbol{R}_n\cdot\boldsymbol{R}_n\rangle = \Big\langle\Big(\sum_{i=1}^{n}\boldsymbol{b}_i\Big)\cdot\Big(\sum_{j=1}^{n}\boldsymbol{b}_j\Big)\Big\rangle, \tag{7}$$

where $\boldsymbol{b}_i$ refers to the bond vector. However, for ring polymers, this quantity cannot work again, because ring polymers have no ends at all. Thus, the radius of gyration is used to characterize the size of the ring polymer. The mean square radius of gyration is defined as the average square distance between monomers

$$\langle R_G^2\rangle = \frac{1}{N}\sum_{i=1}^{N}\langle(\boldsymbol{r}_i - \boldsymbol{r}_{\rm cm})^2\rangle = \frac{1}{N^2}\sum_{i=1}^{N}\sum_{j=1}^{N}\langle(\boldsymbol{r}_i - \boldsymbol{r}_j)^2\rangle, \tag{8}$$

where $\boldsymbol{r}_i$ refers to the monomer position vector, and $\boldsymbol{r}_{\rm cm}$ refers to polymer's center of mass.

To characterize the equilibrium structure of ring polymers, we calculated the mean-square radius of gyration $\langle R_{\rm G}^2\rangle$, the mean-square radius of gyration in the z direction $\langle R_{{\rm G}_z}^2\rangle$, and the average thickness $\langle z\rangle$ defined as

$$\langle z\rangle = \frac{\int_0^{\infty} z\Phi(z)\,{\rm d}z}{\int_0^{z}\Phi(z)\,{\rm d}z}\quad, \tag{9}$$

where $\Phi(z)$ is the volume fraction as a function of the distance from the substrate. The monomer volume fraction in the brush is the statistical average of the contributions of configurations ending up at different positions. It is also called monomer density in this paper. Figure 2 shows the local volume fraction of

monomers for chain length 64, which follows step-like profiles. The extension in brushes is substantially increased with increasing grafting density.

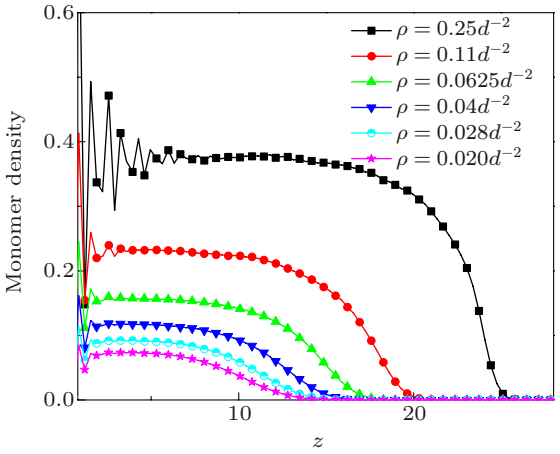

Fig. 2. (color online) Monomer density versus distance from the substrate for ring polymer brush for different grafting densities (64 chains, 64 monomers per chain).

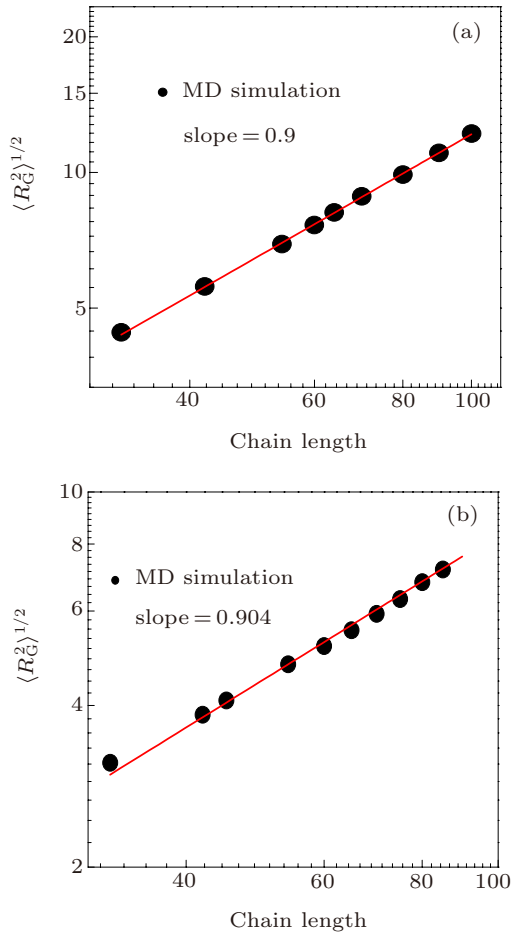

Fig. 3. (color online) The radius of gyration $\langle R_G^2 \rangle^{1/2}$ for (a) linear polymer brush and (b) ring polymer brush versus chain length N at grafting density $\rho = 0.11d^{-2}$.

Both the scaling theory of Alexander[2] and the SCF theory of Milner *et al.*[5] predicted that the height of linear polymer brushes grows with molecular weight and grafting density as $h \sim N\rho^{1/3}$. The simplest description from Alexander assumed that, in the regime of high grafting density ρ, the chains overlap strongly, so that the chains can be treated as linear arrays of blobs (with n monomers in each blob) of diameter $\rho^{-1/2}$, which is the average distance between grafting points. On length scales smaller than the blob size, the chain statistics are unperturbed and the blob size can still employ the statistics law, $\rho^{-1/2} = n^{3/5}$. The blobs in each chain have a number of $n_B = N/n = N\rho^{5/6}$, and so the brush height is the blob size times the number of blobs per chain, i.e., $h \sim N\rho^{1/3}$. For a linear polymer brush, the radius of gyration exhibits the same grafting density scaling law[22] as its height if the prefactor is omitted. To measure the height of a polymer chain, we calculate the radius of gyration for both linear and ring polymers with different chain lengths, as shown in Fig. 3.

Comparison with the scaling law $\langle R_G^2 \rangle^{1/2} \sim N^{\upsilon}$ yields the exponents $\upsilon = 0.90$ and $\upsilon = 0.904$, respectively, for linear polymer brush and ring polymer brush, showing no significant difference of dependence on chain length between the two topological structures. It is a little smaller than theoretical limit $N = 1$. The data for this picture corresponds to grafting density $\rho = 0.11d^{-2}$ and chain length $N = 64$, and so the curves covered both the brush regime and mushroom regime, and yield an exponent less than 1.

In order to investigate how the static properties of different topological structures depend on grafting density, Fig. 4 presents the radius of gyration for a given chain length $N = 64$ at different grafting densities. Two different regimes are also distinguished. The scaling exponent defined by $\langle R_G^2 \rangle^{1/2} \sim \rho^{\nu}$ for ring polymer brushes is $\nu = 0.27$, which is smaller than that for linear polymer brushes $\nu = 1/3$. In the low-density regime, $\rho < \rho^*$, the chains hardly interact with each other, and the polymers in this case form separated mushrooms on the surface. For large grafting density, $\rho > \rho^*$, and the chains are strongly overlapping. Since we assume the solvent to be good, monomers repel each other, and as a result the polymers extend away from the grafting surface. In addition to different power exponents, they also exhibit different turnover grafting densities distinguishing the mushroom regime and the brush regime. The turnover density $\rho^* = 0.07$ for a ring polymer brush is smaller than that for a linear polymer brush, $\rho^* = 0.091$. It can also be found from Fig. 4 that, for a given size N, a ring polymer brush is smaller than a linear polymer brush. The result for linear brush proves the predictions of Alexander and Miler, $h \sim N\rho^{1/3}$. The main conclusion drawn from the investigation of the equilibrium structure of rings in the good solvent is that, for the same chain length and grafting density, the ring polymer brush has smaller size and is more compact than the linear polymer brush, as a result of the effective excluded-volume effect.

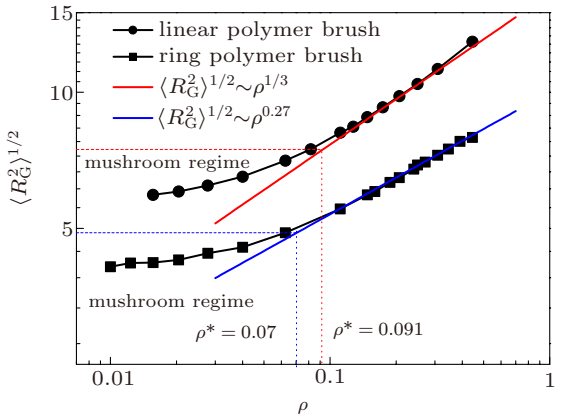

Fig. 4. (color online) The radius of gyration $\langle R_G^2\rangle^{1/2}$ versus grafting density for chain length $N = 64$ (squares for ring polymer brush and circles for linear polymer brush). The $\rho^* = 0.07$ and $\rho^* = 0.091$ characterize the limiting behavior of mushrooms.

In order to characterize the orientation induced by grafting density, we also calculated

$$\langle \cos\theta_i\rangle = \langle (z_i - z_{i-1})/|(\boldsymbol{r}_i - \boldsymbol{r}_{i-1})|\rangle, \tag{10}$$

where θ_i is the angle between the i-th bond and the z axis, $\boldsymbol{r}$ is the monomer position, and $i = 0$ stands for the grafted point of the brush. Figure 5 presents $\langle \cos\theta_i\rangle$ for the i-th monomer along the chain at different grafting densities for linear polymer brush and ring polymer brush. The $\langle \cos\theta_i\rangle$ as a function of chain length is presented in Fig. 6. It is shown in Fig. 5 that $\langle \cos\theta_i\rangle$ for ring polymer brush reveals a symmetrical distribution feature and in the high grafting density regime, the strong interaction between monomers leads to a strong stretch of chains, and as a result a uniform $\langle \cos\theta_i\rangle$ along the chain is obtained. To represent the anisotropy of the bond orientations, the second Legendre polynomial $P_2(\theta) = (3\langle\cos^2\theta\rangle - 1)/2$ is also calculated. A positive value of P_2 $(0 \le P_2(\theta) \le 1)$ means a preference of the bonds to orient perpendicularly to the substrate, while $P_2(\theta) = 0$ means that the orientations are more likely to take random distribution. Figure 7 plots the distribution of orientation $P_2(\theta)$ of bonds along the chain. The orientations for ring and linear brushes are both negative $(-1/2 \le P_2(\theta) \le 0)$ in the mushroom regime at low grafting density, in which chains tend to collapse and extend parallel to the grafting surface. The $P_2(\theta)$ for the end monomer in linear brush simulations is always close to zero, indicating that the free ends are randomly distributed inside the brush. In ring polymer brush simulations, we also find free bond orientation $P_2(\theta) = 0$ like free ends in a linear brush.

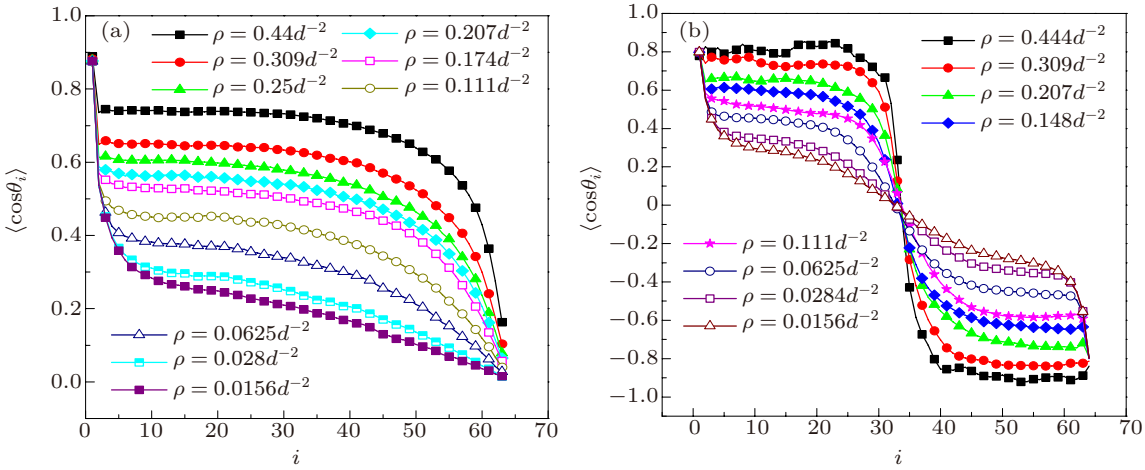

Fig. 5. (color online) $\langle \cos\theta_i\rangle$ for the i-th monomer along the chain at different grafting densities for chain length $N = 64$. (a) Linear polymer brush, (b) ring polymer brush.

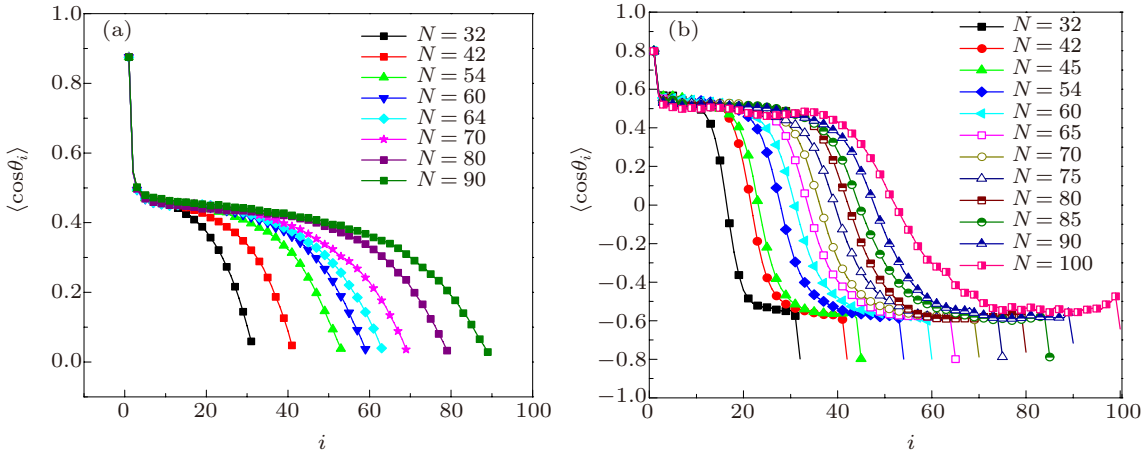

Fig. 6. (color online) $\langle \cos\theta_i\rangle$ for the i-th monomer along the chain as a function of chain length. (a) Linear polymer brush, (b) ring polymer brush.

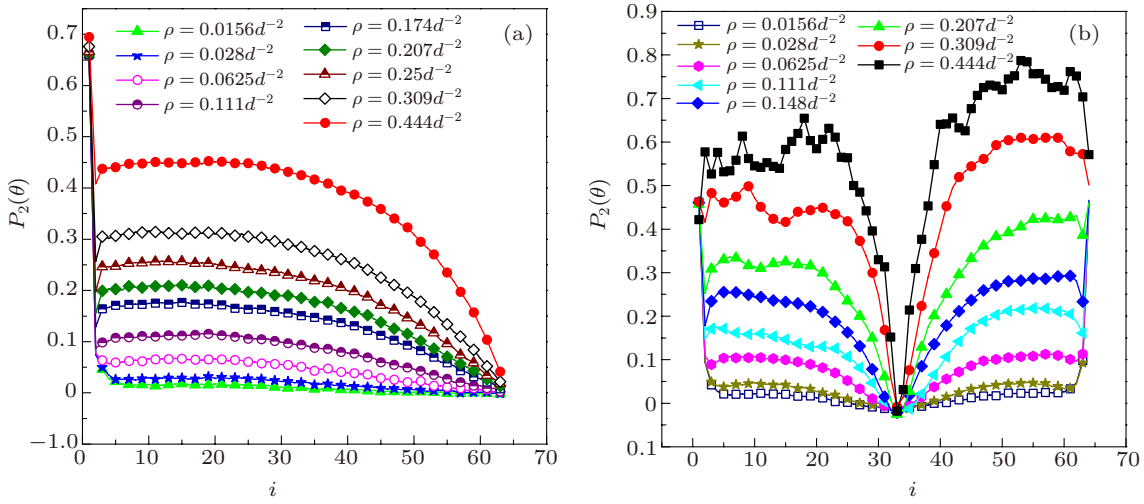

Fig. 7. (color online) Average bond orientations $P_2(\theta)$ versus the bond sequential number i for chain length $N = 64$ at different grafting densities. (a) Linear polymer brush, (b) ring polymer brush.

3.2. Bond force and chain energy

As monomers tie together to form polymers via a covalent bond, it is also of interest to explore their bond forces. Starting from the FENE bond style defined by Eq. 3, the bond force along the bond vector is given by

$$\boldsymbol{F} = \langle \nabla U_{\mathrm{FENE}}(\boldsymbol{b}) \rangle = \left\langle -\boldsymbol{b}\left(\frac{kB^2}{b^2 - B^2} + \frac{4\varepsilon}{b^2}\left[12\left(\frac{d}{b}\right)^{12} - 6\left(\frac{d}{b}\right)^{6} \right] \right) \right\rangle. \quad (11)$$

Figure 8 shows the z component of the bond force. At the end of the linear brush, the z-component force is close to zero when the grafting density is not high enough. On the contrary, in a high grafting density regime, the end bond still exhibits strong stretching due to the strong interaction of its neighboring monomers. In the ring polymer brush, the z-component force is distributed symmetrically. On the top of the ring polymer brush, the z-component force vanishes. The first bond, which connects the grafted monomer and the the first movable monomer, shows particularly high stretching force in both ring and linear polymer brushes.

The stretching energy of each chain is obtained by integrating the force along the z direction. As in Alexander's assumption, each chain is a stretched array of tension blobs. The blob size is the length scale on which the cumulative interaction energy is of the order of thermal energy $k_{\mathrm{B}}T$. The total stretching energy per chain is $k_{\mathrm{B}}T$ times the number of the blobs. According to the derivation in Section 3.1, i.e., $n_{\mathrm{B}} = N\rho^{5/6}$, we obtain

$$F_{\mathrm{ene}} \sim k_{\mathrm{B}}T, \quad (12)$$

where F_{ene} is the stretching energy. In Fig. 9, the stretching energy scaled by chain length N is presented both for linear and ring polymer brush. In agreement with Eq. 12, the profiles with different chain length can converge into one master profile with a scaling exponent $\nu = 0.81$ for linear polymer brush in moderate and high grafting density. However, a smaller exponent $\nu = 0.73$ is found for ring polymer brush. The two curves both shift away from the power scaling law in a mushroom regime.

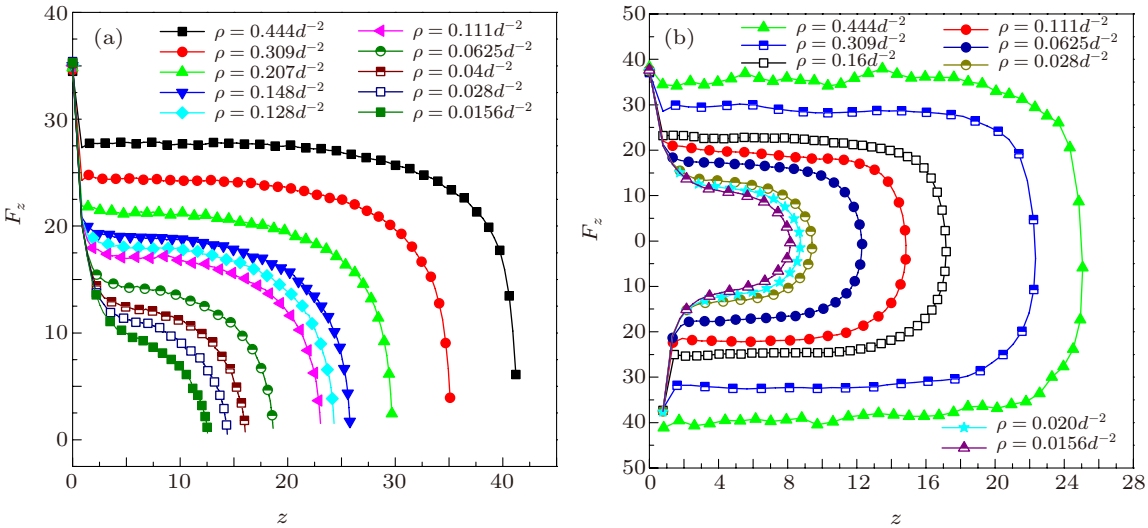

Fig. 8. (color online) Averaged bond forces along the z direction as a function of the distance from the surface. (a) Linear polymer brush for $N = 64$, (b) ring polymer brush for $N = 64$.

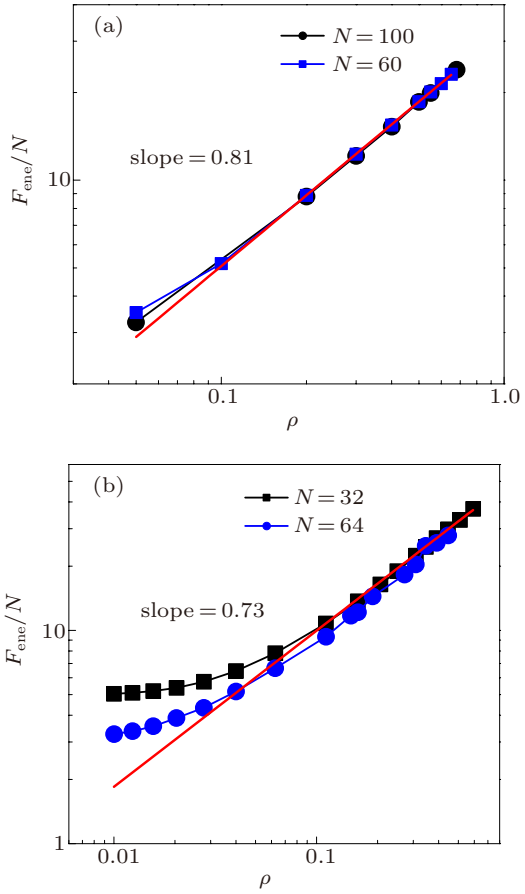

Fig. 9. (color online) Stretching energy scaled with N as a function of grafting density. (a) Linear polymer brushes with $N = 60$ and $N = 100$, (b) ring polymer brushes with $N = 32$ and $N = 64$.

4. Results for long chains ($N = 128, 200$)

In the previous sections, results for moderate chain length are presented, and it is shown that ring polymer brushes exhibit different behaviors from those of liner polymer brushes. Figure 10 shows the radius gyration and its z component for chain length of 90, from which we still see a different power exponent 0.27 for the z component of radius gyration of ring polymer brush rather than $1/3$. As in moderate long chain length, the ring polymer chain can be treated as two equivalent linear chains. It can be predicted that if the chain length is long enough, the stretching of the ring polymer brush is very strong and the expansion in the z direction is much greater than x–y direction, which will make the ring polymer brushes behave very much like linear brushes.

Figure 11 shows the height profiles against grafting density for $N = 128$, where it is found that for both ring and linear polymer brushes, the radius gyration and radius gyration in the z direction behave very closely with the same power law index 0.38 against grafting density, compared with theoretical prediction $1/3$. The difference is caused by bond and Kuhn length fluctuations in MD simulations.

The total stretching energy as a function of grafting densities for chain length $N = 128$ shown in Fig. 12 also exhibits the same scaling behavior between the two topological structures.

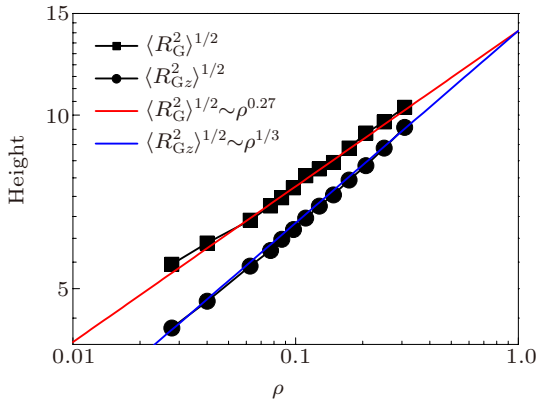

Fig. 10. (color online) The radius of gyration $\langle R_G^2 \rangle^{1/2}$ and its z component $\langle R_{G_z}^2 \rangle^{1/2}$ versus grafting density for ring polymer brush with $N = 90$.

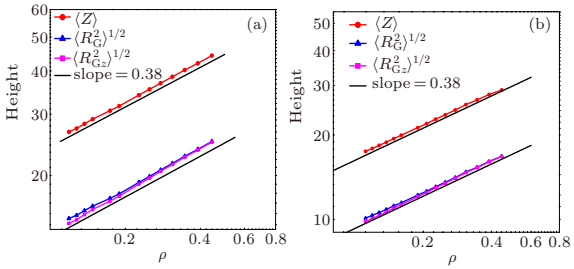

Fig. 11. (color online) Radius of gyration $\langle R_G^2 \rangle^{1/2}$, radius of gyration in the z direction $\langle R_{G_z}^2 \rangle^{1/2}$ versus the grafting density for $N = 128$.

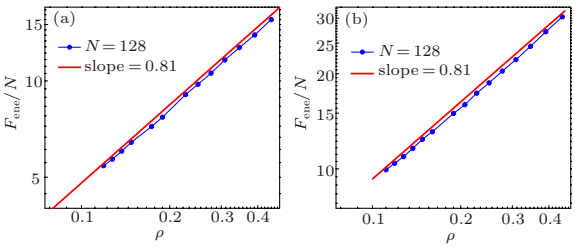

Fig. 12. (color online) Stretching energy scaled with N as a function of grafting density. (a) Linear polymer brush, (b) ring polymer brush.

In Fig. 13, after the horizontal coordinates are scaled by $\rho^{-1/3}$ and the monomer densities by $\rho^{-2/3}$, the profiles of monomer density perfectly fall into a master curve both for linear and ring polymer brush. However, it is found from Fig. 13 that the density distribution for ring polymer is more step-like, as ring polymer brush is more crowded than linear polymer brush at the same grafting density and chain length.

It can be concluded that a ring polymer brush will behave like a linear polymer brush if the chain length is long enough, which can also be supported by the results of chain length $N = 200$, as shown in Figs. 14 and 15, revealing the same behaviors as $N = 128$.

The reason why the AdG model cannot be successfully applied for a ring polymer brush for moderate or small chain length is that ring polymer brushes have enough extension in

both x and y directions, and the blobs around the top position are not independent of each other. The SCF model will become invalid in this regime due to the non-uniform monomer distribution (and thus strong fluctuation) in $x-y$ surface. If the chain length is much longer than the surface lattice length, the $x-y$ distribution effects can be omitted, and consequently ring polymer brushes will reveal the same behaviors as those of linear polymer brushes.

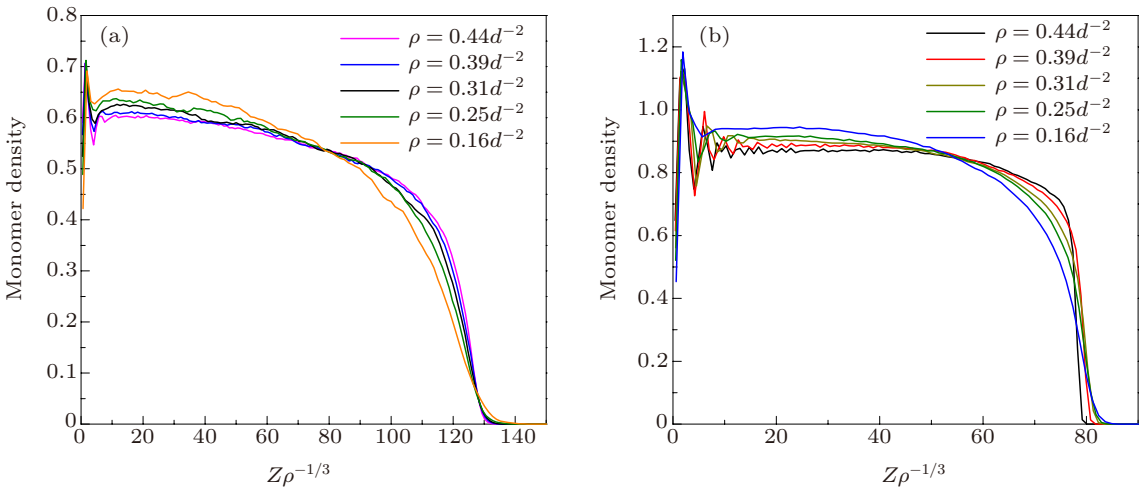

Fig. 13. (color online) Rescaled monomer density versus rescaled distance from grafting surface for different grafting densities with $N = 128$. (a) Linear polymer brush, (b) ring polymer brush.

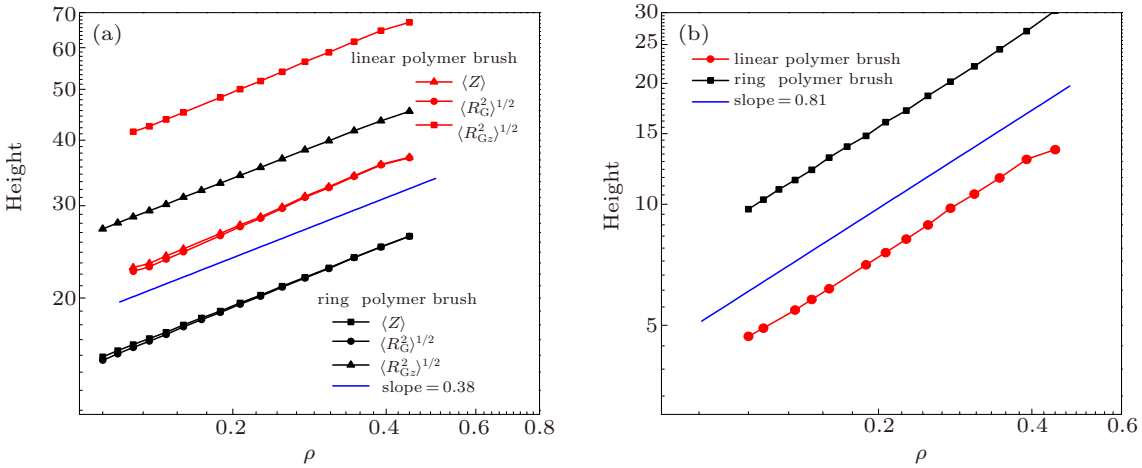

Fig. 14. (color online) Simulation results for a ring polymer brush with $N = 200$. (a) Central height $\langle z\rangle$, radius of gyration $\langle R_G^2\rangle^{1/2}$, radius of gyration in the z direction $\langle R_{G_z}^2\rangle^{1/2}$ versus the grafting density, (b) stretching energy scaled by N as a function of grafting density.

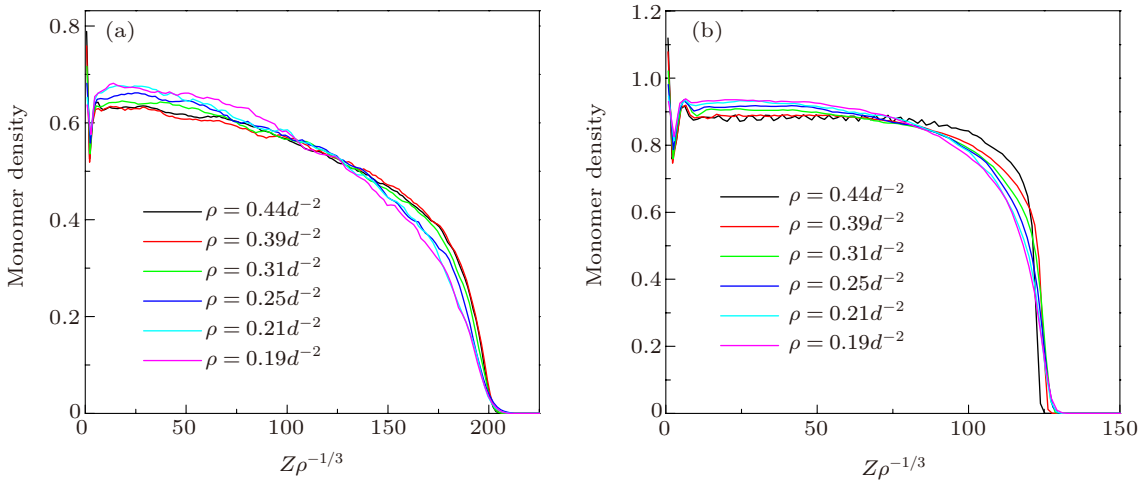

Fig. 15. (color online) Rescaled monomer density by $\rho^{-2/3}$ versus rescaled distance by $\rho^{-1/3}$ from grafting surface for different grafting densities with $N = 200$. (a) Linear polymer brush, (b) ring polymer brush.

5. Conclusions

In this paper, we present a detailed MD simulation study of an end-grafted ring polymer brush in good solvent. The average static and dynamic quantities of ring polymer brushes are examined and compared with those of linear polymer brushes. It is found that the thickness of a ring polymer brush reveals a power scaling law of $h \sim N\rho^{0.27}$ rather than $h \sim N\rho^{1/3}$ for a linear polymer brush for moderate chain length, indicating that the scaling law depends on topological features in this regime. A study of the average equilibrium structure quantities like bond orientation shows that at high grafting density, the last bond tension still exits in linear brush, but for a ring polymer brush, the bond force vanishes at the brush top. This is due to its symmetrical distributions of $\langle \cos\theta_i \rangle$ and its characteristics are confirmed by bond force F_z. The total stretching energy scaled by chain length N in moderate chain length regime has the master scaling power law, $F_{\text{ene}} \sim N\rho^{0.81}$ for linear brushes, and $F_{\text{ene}} \sim N\rho^{0.73}$ for ring polymer brushes. Due to the long chain length, the extension in the z direction is much stronger than x–y direction, which makes ring polymer brushes behave like linear polymer brushes, and thus deliver the same power laws, such as $h \sim N\rho^{0.38}$ for thickness and $F_{\text{ene}} \sim N\rho^{0.81}$ for total stretching energy. The rescaled monomer density also falls into a master curve.

References

[1] Netz R R and Schick M 1998 *Macromlecules.* **31** 5105
[2] Alexander S 1977 *J. Phys.* **38** 977
[3] de Gennes P G 1980 *Macromolecules.* **13** 1069
[4] Semenov A N 1985 *Sov. Phys. JETP* **61** 733
[5] Milner S T, Witten T A and Cates M 1988 *Macromolecules.* **21** 2610
[6] Wijmans C M, Scheutjens J M H M and Zhulina E B 1992 *Macromolecules* **25** 2657
[7] Amoskov V M and Pryamitsyn V A 1994 *J. Chem. Soc. Faraday Trans.* **90** 889
[8] Shim D F K and Cates M E 1989 *J. Phys.* **50** 3535
[9] Borisov O V, Leermakers F A M, Fleer G J and Zhulina E B 2001 *J. Chem. Phys.* **114** 7700
[10] Biesheuvel P M, de Vos W M and Amoskov V M 2008 *Macromolecules.* **41** 6254
[11] Matsen M W 2004 *J. Chem. Phys.* **121** 1938
[12] Lai P Y and Halperin A 1991 *Macromolecules.* **24** 4981
[13] He S Z, Merlitz H, Chen L, Sommer J U and Wu C X 2010 *Macromolecules.* **43** 7845
[14] Chen L, Merlitz H, He S Z, Sommer J U and Wu C X 2011 *Macromolecules.* **44** 3109
[15] Zhang L X and Shen Y 2008 *Chin. Phys. B.* **17** 1480
[16] Hur K, Winkler R G and Yoon D Y 2006 *Macromolecules.* **39** 3975
[17] Klein A 1990 *Macromolecules.* **23** 2984
[18] Di Marzio E A 1993 *Macromolecules.* **26** 4613
[19] Stratouras G K and Kosmas M K 1991 *Macromolecules.* **24** 6754
[20] Plimpton S J 1995 *J. Comput. Phys.* **117** 1
[21] Kremer K 1990 *J. Chem. Phys.* **92** 5057
[22] Halperin A, Tirrell M and Lodge T 1992 *Adv. Polym. Sci.* **100** 31